Designing Optimized Antennas for Science Applications Using Evolutionary Algorithms

Julie Rolla,* **Bryan Reynolds,†** **Jacob Weiler,†** **Dylan Wells,†** **Max Foreback,‡** **Amy Connolly,†** **Emily Dolson,‡** **and Charles Ofria‡**

ABSTRACT. — This report presents developments to a genetic algorithm that evolves antenna designs from primitive shapes. The gain patterns of individuals are evaluated using XFdtd electromagnetic simulation software and fitness is evaluated by integrating in a novel Monte Carlo simulation software assessing the performance of the designs in a science environment. This work is an update to a prior report demonstrating evolution of dipole-like antennas with a fitness focused on convergences to similar gain patterns or features in antenna performance. In this report we show the algorithm is capable of designing dipole-like antennas optimized for specific performance metrics based on simulation software for science experiments. The algorithm was updated to incorporate an age-layered population structure to improve convergence and computational efficiency. This report presents initial results on an improved antenna design for an in-ice neutrino detector using the simulation software of the Askaryan Radio Array (ARA) experiment as a proof-of-concept. Several additional design features allowing for reflectors and multi-feed are currently in the testing phase and will also be briefly discussed.

I. Introduction

This report presents an evolutionary algorithm that evolves three-dimensional antenna designs from primitive shapes to produce specified gain patterns *without* predefined antenna topologies (e.g., dipole or biconical). This work expands upon the previous Interplanetary Network Progress Reports "Design of 3D Antenna Geometries Using

*Tracking System and Applications Section.

†Department of Physics, Center for Cosmology and AstroParticle Physics, The Ohio State University.

‡Department of Computer Science and Engineering, Michigan State University.

The research described in this publication was carried out by the Jet Propulsion Laboratory, California Institute of Technology, under a contract with the National Aeronautics and Space Administration.

Genetic Algorithms" (August 2023) and "Design of Antennas from Primitive Shapes Using Genetic Algorithms" (May 2024). The first report detailed the method for evolving 3D structures using evolutionary algorithms (EAs) and displayed the algorithm's ability to evolve toward a target geometric design [1]. The second report discussed further developments to the algorithm that allowed for the evolved structures to be treated as antennas, including the placement of a voltage feed, prevention of unwanted electrical shorting in the evolved designs, and the integration of XFdtd, an electromagnetic finite difference in the time domain simulation software developed by Remcom Inc. [2], with the EA to produce simulated antenna gain patterns. It was verified that the algorithm is capable of evolving toward designs that achieve specified target gain and phase patterns, as well as toward designs that maximize or minimize sensitivity in specified directions, for both single-frequency and broadband cases [3].

The previous reports demonstrated an algorithm capable of creating 3D structures that function as single-feed, dipole-like antennas, marking initial steps toward the wider goal of designing antennas optimized for specific scientific outcomes. The method consisted of assembling geometric primitives according to rules of construction and evaluating the fitness of the created structures using cost functions devised to represent the antenna design's similarity to a target antenna beam pattern or degree of sensitivity in specified directions.

The work presented in this report includes further developments to the algorithm, namely the implementation of cost functions in the EA that are derived from performance metrics based on science simulation software. The AraSim [4] software is used as an example to demonstrate the evolution of antennas toward a desired science outcome. Several enhancements to the EA were also made to improve the speed of converging to a high-quality solution and consequently reduce computation time, which becomes increasingly necessary as more complex antenna designs are considered. Future versions of the algorithm will evolve toward complex science goals by broadening its capabilities to generate antennas with more complex designs efficiently.

The complex, high-dimensional parameter spaces involved in the design and optimization of detectors motivate the use of a heuristic to aid the initial design phase. Heuristic techniques, such as evolutionary algorithms, are effective at uncovering high-quality solutions to problems involving high-dimensional parameter spaces, as encountered in antenna design [5]. By allowing for the ability to efficiently approximate an optimal solution without evaluating all potential solutions, computation efficiency is greatly increased compared to a comprehensive grid search method.

This report examines the application of EAs to design antennas optimized for specific performance metrics based on simulation software for science experiments. Although this approach has the potential to extend to a wide variety of detector technologies, the initial focus is on increasing sensitivity for radio observations, including antennas for the Global Navigation Satellite System (GNSS) [6, 7, 8], passive

sounding [9, 10, 11], and low-frequency radio astronomy, encompassing signals such as those from extrasolar planets [12, 13, 14], cosmic ray electrons and cosmic magnetic fields [15, 16, 17, 18, 19], and the highly redshifted neutral hydrogen hyperfine line [20, 21, 22, 23]. By addressing a critical need for innovative emerging design optimization tools, this work seeks to enhance the scientific reach of future astrophysics experiments, ranging from instrumentation for flagship missions to low-cost SmallSats, which must meet complex performance, geometric, and budgetary specifications. Planned future efforts focusing on multi-objective optimization (MOO) to account for the numerous and potentially competing objectives influencing antennas and hardware required for mission design will also further these goals.

Evolutionary algorithms have been successfully applied across various domains, including antenna design, and continue to be the focus of ongoing research [24, 25, 26, 27, 28]. Recent developments in the use of EAs for antenna array optimization have further advanced this field [29, 30, 31]. While prior work shows the successful use of EAs to fine-tune and optimize engineered antenna designs for science outcomes [32, 33], this work aims to automate the *de novo* design of antennas. To do so, the algorithm employs a steady-state EA that constructs and evolves antenna geometries built using primitive shapes, similar to modular building block components [1].

This report presents initial findings resulting from the use of an EA to construct antennas and evolve designs optimized based on performance in science simulations as a measure of fitness. The algorithm has been updated to evolve using an age-layered population structure (ALPS), which keeps multiple sub-populations of different ages partially separated from each other to reduce premature and sub-optimal convergence [34, 35]. ALPS reduces premature convergence and more effectively explores the parameter landscape by allowing new individuals with new traits to evolve without being dominated by old high-fitness individuals.

As an introductory test application, this paper presents initial results of an evolutionary algorithm designing optimized antennas using results from science simulation software, as the sole measure of fitness. With this study, we aim to provide a proof of concept for using EAs that construct antennas from primitive shapes, to design more sensitive detectors for science outcomes.

Section II describes a detailed overview of the EA, including the construction of individuals, XFdtd simulations, fitness evaluation, and the selection methods and operators used. Section II.C describes the process of calculating fitness scores that were utilized in the evolution. The results of the evolution are presented in Section III and discussed in Section IV. Finally, Section V discusses the significance of the results, the next steps in evolving antenna designs toward specified science outcomes, planned and in progress future work, and potential challenges identified.

II. The Evolutionary Algorithm

A schematic diagram of the EA developed for this analysis is depicted in Figure 1. The algorithm begins by generating an initial population of individuals according to the steps discussed in Section II.A. Those designs are then modeled in XFdtd, which simulates the antenna gain pattern of each individual. This allows a fitness score to be assigned to each individual based on their performance in a science simulation that utilizes their simulated antenna gain patterns. The efforts reported here specifically focus on optimization of the vertically polarized Askaryan Radio Array (ARA) antenna design, evaluating individual performance using simulation software. The fitness scores based on this performance are then used to select parents and create offspring. The fitness function calculations are discussed in detail in Section II.C.2. The EA has a number of parameters that may vary depending on the types of primitives used in each design, which are summarized in Appendix I.

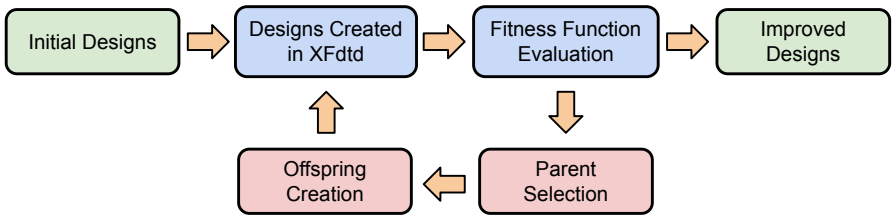

Figure 1. Diagram illustrating the basic loop of the EA. Green boxes indicate initialization and termination. The blue boxes show the steps required to evaluate the fitness function, and the red boxes indicate the steps for creating the new individuals.

A. Building an Evolvable 3D Antenna

Creating a potential antenna design that can be evolved as part of an EA is a non-trivial problem. Individuals in our algorithm are composed of four basic geometric primitive shapes: cuboids, cylinders, cones, and spheres. Primitives act as building blocks connected to each other to form a more complex structure, as illustrated in Figure 2. Multiple primitives of the same shape can be used in an antenna design, and there are no requirements that any specific shape be used. An individual is fully described by a tree structure that describes the dimensions, location, orientation, and connections of each component shape. Each primitive type is given a specified range of values in which its dimension and rotation genes must exist. Table 1 shows the genes and their specified ranges for each primitive type used here. To streamline construction of individuals, a number of constraints are imposed. First, all shape types behave consistently, with a single attachment point in each region corresponding to its front, back, left, right, top, and bottom. Additionally, when cylinders and cones are added to another shape, they always connect with their flat top or bottom face, although other shapes can be added to the curved surfaces. Specific to the use case of optimizing the ARA vertically polarized antenna design, another constraint requires that the created designs fit into the 15 cm borehole currently being used. Operations

that lead to designs that do not fit within this size constraint are disallowed. Lastly, for the efforts discussed in this report, individuals were allowed to contain up to seven primitive shapes. A more comprehensive discussion of the basic methodology for individual construction is given in previous manuscripts [1, 3].

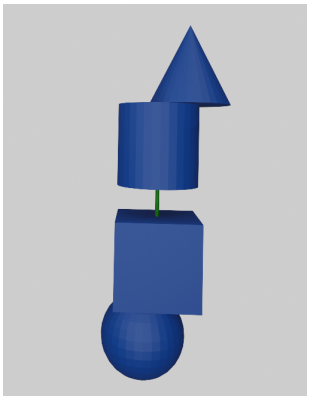

Figure 2. Example individual consisting of each of the four primitive shapes.

In order for an individual to function as an antenna, the voltage feed and grounding point must be incorporated into the design. The algorithm currently constructs single-feed dipole-like antenna designs, starting each candidate solution with one primitive attached to the antenna feed line and another primitive to the ground. For each individual, a small cube is generated at the origin as a placeholder for the antenna feed and ground assemblies, and is replaced by those structures when the design is simulated as an antenna. Each individual construction begins by attaching two shapes to the initial cuboid. Next, there is a breadth-first placement of new shapes, where between one and five new shapes are attached to open sides on an already placed shape. This process is repeated in layers, starting with the initial two shapes and moving outward until the individual reaches a maximum shape count or branch depth.

To prevent potential antenna performance issues caused by shorting across the feed point, a collision detection algorithm was implemented using the open source Flexible Collision Library software package [36]. Each time a new primitive is added or the genes of an existing primitive are changed, the algorithm disallows any operations that cause overlap between primitives that are electrically connected to opposite sides of the feed point. We acknowledge that universally disallowing shorting limits the potential antenna designs that the algorithm may create; however, this restriction is suitable for the single-feed dipole-like cases that are the focus of this report.

B. Initialization

The population is initialized through the construction of individuals with randomized genes. For this analysis, each individual must have between 3 and 7 shapes, including the starting cube that is eventually replaced by the voltage feed.

Table 1. Genes of each primitive.

Gene	Minimum	Maximum
Primitive Type: Cylinder		
Height (cm)	10.0	140
Radius (cm)	0.31	7.5
Theta (deg)	-90	90
Phi (deg)	-90	90
Midpoint Coordinates	*	*
Primitive Type: Cuboid		
Length (cm)	0.62	15
Width (cm)	0.62	15
Height (cm)	0.62	140
Theta (deg)	-90	90
Phi (deg)	-90	90
Midpoint Coordinates	*	*
Primitive Type: Sphere		
Radius (cm)	2.0	7.5
Theta (deg)	-90	90
Phi (deg)	-90	90
Midpoint Coordinates	*	*
Primitive Type: Cone		
R1 (cm)	0.31	7.5
R2 (cm)	0.31	7.5
Height (cm)	10	140
Theta (deg)	-90	90
Phi (deg)	-90	90
Midpoint Coordinates	*	*

*Midpoint coordinates are constrained by prior shapes' coordinates.

C. Fitness Calculation

Once an individual is defined, the fitness score must be determined in order to select parents for the creation of future individuals. To calculate fitness scores, gain patterns are first simulated in XFdtd. Subsequently, the science simulation software uses these gain patterns to determine the sensitivity of the individual to Ultra High Energy (UHE) neutrinos [4]. The calculations of the fitness score are computationally expensive and require the use of a supercomputer cluster. The fitness calculation is parallelized across up to 200 different processes per individual, allowing for an

individual evaluation to be completed in approximately five minutes. Multiple individuals are tested simultaneously, and thus, an individual completes the evaluation step approximately every minute on average. The steps in determining an individual's fitness score are discussed in depth in the following sections.

1. Creating Antennas in XFdtd

The dictionary corresponding to an individual's tree structure is used to construct a model in XFdtd through the program's scripting interface. For this study, all primitives were modeled as hollow and represented by perfect electrical conductor material. The algorithm allows for single frequency or broadband analysis, with the latter performed with a series of simulations at individual frequency steps within a defined range.

For this work, a broadband frequency range was used, incorporating 37 different frequencies of equal steps from 200 MHz to 800 MHz. The antenna response was simulated at 5° increments of the azimuth-zenith coordinates.

The gain of an antenna is a measure of how efficiently it converts received radio waves from a given direction into power. XFdtd calculates the far-field realized gain (hereafter referred to as simply "gain") of an antenna at a specific (θ, ϕ) coordinate using Eq. 1 [37]:

$$G_{\mathrm{R}} \;=\; \frac{2\pi r^2 |\widetilde{E}(\theta,\phi)|^2}{\eta P_{\mathrm{M}}} \;. \tag{1}$$

Here, G_{R} is the realized gain [38] of the antenna in a specific direction in dBi. $\widetilde{E}(\theta,\phi)$ is the complex electric field incident on the antenna from the (θ,ϕ) direction, η is the wave impedance in the medium (377 Ω in free space), r is the distance between the power source and the sensors in the simulation (1 m), and P_M is the power accepted by the antenna. The gain is equivalent to the directivity multiplied by the antenna's radiation efficiency.

2. Antenna Sensitivity

The Monte Carlo simulation program intakes the gain patterns generated by XFdtd to simulate the performance of the individual [4].

To calculate the fitness score, the sensitivity, known as the effective volume ($[V\Omega]_{\mathrm{eff}}$), is simulated when the evolved antenna is used. Effective volume is directly proportional to the number of detected events, making it an appropriate fitness score to be used by the EA. The effective volume $[V\Omega]_{\mathrm{eff}}$ is given by:

$$\text{Fitness Score} = [\mathrm{V}\Omega]_{\mathrm{eff}} \;=\; 4\pi\ \mathrm{V}_{\mathrm{ice}}\ \frac{\mathrm{N}_{\mathrm{detected}}}{\mathrm{N}_{\mathrm{simulated}}} \tag{2}$$

where V_{ice} is the volume of ice simulated, N_{detected} is the number of events detected, and $N_{\text{simulated}}$ is the number of simulated events [39]. For this work, 1.2×10^6 events are simulated, which results in an effective volume standard deviation of approximately $0.2\,\text{km}^3\text{sr}$.

Due to the uncertainty inherent in the simulation software, the algorithm may struggle to effectively fine tune the oldest, most elite solutions. To remedy this, after approximately 6000 evaluations, the number of simulated neutrinos thrown was increased to 3×10^6, and all individuals were re-simulated. While this change was computationally costly, it caused a sharp increase in selection pressure, and meant that the EA could more accurately identify the best solutions in the population for fine tuning.

D. Generating New Individuals

Tournament selection is used with the steady state algorithm to select the parent individuals that will produce a new child. In tournament selection, a random subset of T individuals is selected, and the one with the highest fitness score is chosen as a parent [40, 41]. Here, T is set to 7% of the population to create a relatively strong selection in favor of the current best individuals. The process is repeated each time a parent is needed.

The algorithm uses three main types of operators to build the next generation: mutation, crossover, and injection [3].

Two different types of mutation were implemented: standard mutation and regenerative mutation. In standard mutation, a single dimension, rotation, or location gene for a single shape is altered. A replacement value is drawn from a Gaussian distribution centered on the original value with a standard deviation specified as a percentage of the total range of values. While standard mutation makes minor changes to individuals, regenerative mutation allows larger changes to occur. There are four types of regenerative mutation: grow, prune, replace, and side switch. For grow mutations, an empty side of one shape on the individual is selected, and a new shape is generated that connects to that side. In prune mutations, a shape, and all subsequent connected shapes in the tree, are removed from the individual. Replace mutations exchange one shape with another, where the new shape is generated from scratch. The new shape is constrained to have dimensions that are similar to the shape it is replacing. Finally, side switch mutation selects a shape and moves it, and all subsequent connected shapes in the tree, to a different unoccupied surface of the shape to which it was originally connected.

In the gene and branch crossover operators, components of two parents are combined to produce two offspring. In gene crossover, two parents exchange a single gene of one

shape. The shapes are restricted to be the same type, unless the gene swapped is rotation or location. In branch crossover, all shapes in one branch of the tree structure are swapped between the two parents. The algorithm selects a shape and surface in each of the parents and then exchanges the subtrees rooted at those points. A branch is allowed to be empty, which would effectively prune the branch of the other parent. As with mutation, the algorithm ensures that the shape is still valid and that the constraints are still satisfied following any crossover operation.

Injection is the creation of a brand new individual using the initialization methodology. Due to the ALPS technique, 120 individuals are produced through injection for every 1000 individuals created through the normal evolution.

E. Loop and Termination

The EA continues to iterate and generate individuals using the evolutionary pressure from the AraSim simulations. In this analysis, the EA was run until approximately 10000 individuals had been created, at which point it was manually terminated.

III. Results

The evolution results are presented in Figure 3, with the horizontal dashed line showing the fitness of the current ARA design. During the course of evolution, the highest performing newly created individuals had increasing fitness scores as the run progressed, demonstrating a clear evolution toward improved solutions. To investigate trends in the age layers of the ALPS algorithm, the color of the point represents the age layer in which each individual exists. Dark blue indicates individuals in age layer 1, which are the youngest individuals in the population. Light blue indicates individuals in age layer 2, the intermediately aged portion of the population. Red indicates individuals in age layer 3, the oldest group in the population. This color scheme also illustrates the ALPS technique, as after every approximately every 1000 evaluations, 120 new individuals are created by injection as a new layer, as can be seen in the dark blue points. This new layer has a wide spread of initial fitness scores as individuals are created from scratch without using prior genetic material. The fitness scores of individuals in the new layer quickly evolves to similar levels as the older layers, but typically, younger individuals have lower fitness scores. The vertical dashed line indicates the point at which the number of neutrinos simulated when evaluating each individual was increased from 1.2×10^6 to 3×10^6.

Figure 4 provides an alternative visualization of the evolution, showing the highest fitness score in each age layer created in each generation. Here, a generation is defined as a grouping of 120 individuals. As expected, the most fit individuals tend to exist in age layer 3, the oldest individuals in the population, with age layer 1 exhibiting more variance in the performance of its sub-population. Again, a horizontal dashed line indicates the fitness score of the current ARA antenna design, and a vertical dashed

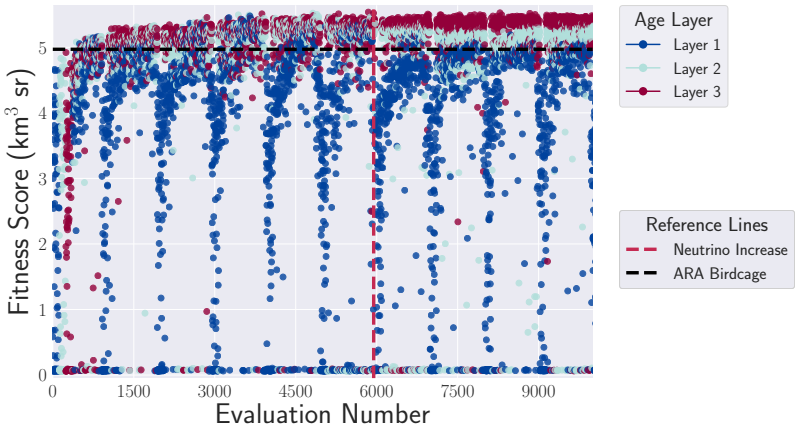

Figure 3. The fitness score of each individual throughout the evolution. The color of the points represents the age layer of the individual. The fitness score of the ARA bicone design is included for comparison, indicated by the horizontal dashed line. The point when the number of simulated neutrinos was increased is indicated by the vertical dashed line.

line shows the point at which the number of neutrinos simulated when evaluating each individual was increased. Fitness scores tend to see a slight decline after the number of simulated neutrinos is increased as individuals are reevaluated with a lower uncertainty, reducing the chances of statistical fluctuations creating unexpectedly high fitness scores. More discussion about the effects of uncertainty on the fitness score is provided in Section IV.

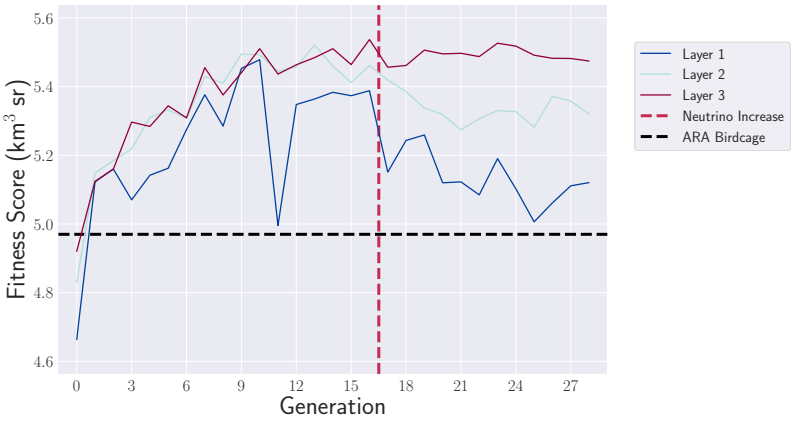

Figure 4. The fitness score of the highest performing individual in each age layer of the population throughout the evolution. The fitness score of the ARA bicone design is indicated by the horizontal dashed line. The point when the number of simulated neutrinos was increased is indicated by the vertical dashed line.

CAD models of the most fit individuals at various stages of evolution are shown in Figure 5. The algorithm quickly discovered designs similar to asymmetric biconical antennas and improved upon them throughout the evolution, adding an extra

primitive and mutating dimension and rotation genes.

(a) Generation 0 Evaluation 244 **(b) Generation 10 Evaluation 3636** **(c) Generation 23 Evaluation 8285**

Figure 5. Three example models representing the most fit individuals at various stages of the evolution.

Gain patterns corresponding to the three selected individuals in Figure 5 are shown in Figure 6, Figure 7, and Figure 8 for frequencies of 300 MHz, 600 MHz, and 900 MHz respectively. Additional gain patterns at the remaining 100 MHz increments between 200 MHz and 1000 MHz are shown in Appendix II. The gain patterns of the evolved antenna designs are shown as green dashed lines and are compared against the gain patterns of the current ARA antenna design, shown with pink diamonds. The highest performing evolved individuals targeted sensitivity in directions that neutrinos are most commonly expected to arrive from, as discussed further in Section III.A.

Table 2. Evolution results.

Individual #	**Primitives**	**Score (km^3sr)**
8369	Branch 1: Cuboid Branch 2: Cylinder	5.613 ± 0.1
8565	Branch 1: Cuboid Branch 2: Cylinder	5.557 ± 0.1
8779	Branch 1: Cuboid Branch 2: Cylinder	5.464 ± 0.1
10884	Branch 1: Cuboid Branch 2: Cylinder	5.459 ± 0.1
8083	Branch 1: Cylinder Branch 2: Cylinder	5.442 ± 0.1

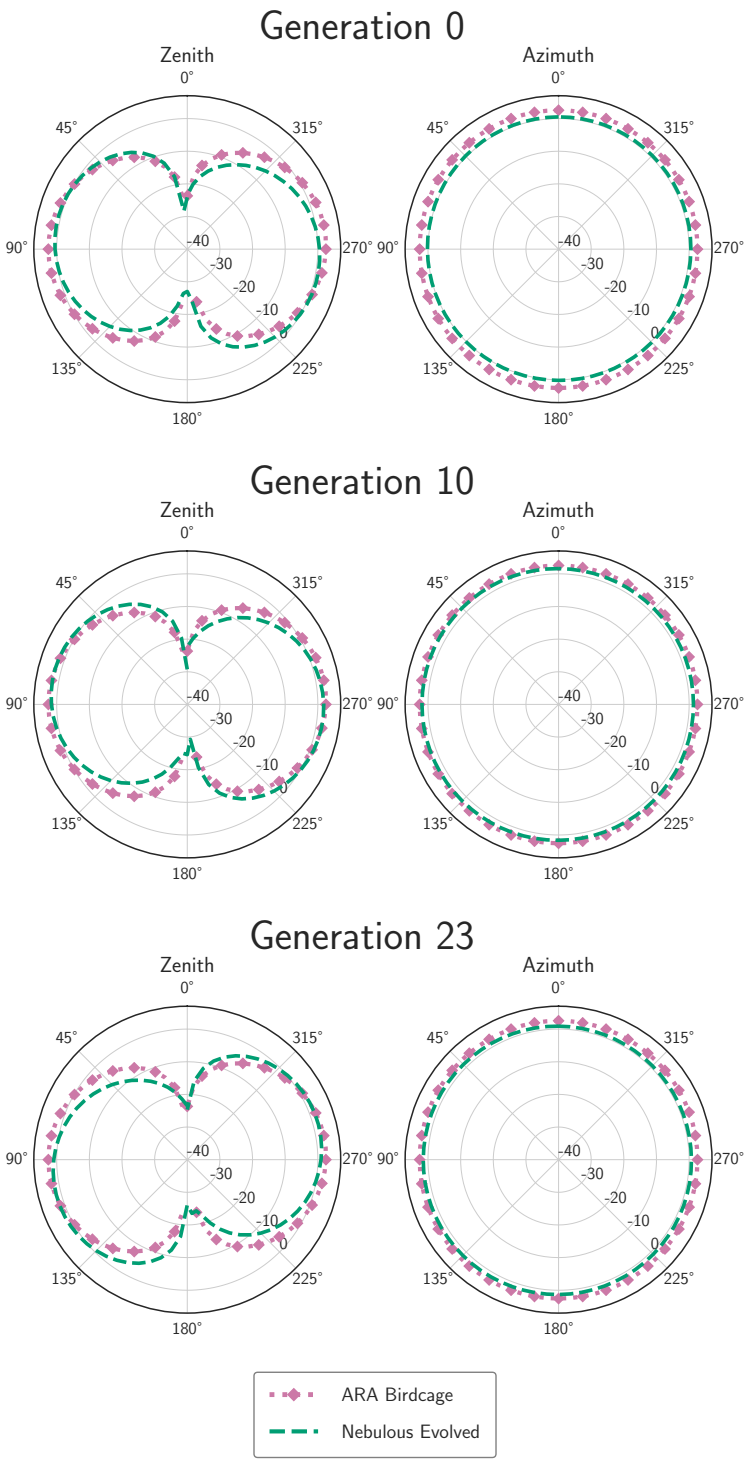

Figure 6. The gain patterns at 300 MHz of the most fit individual as of generations 0 (top), 10 (middle), and 23 (bottom). The ARA antenna gain pattern is overlaid in pink.

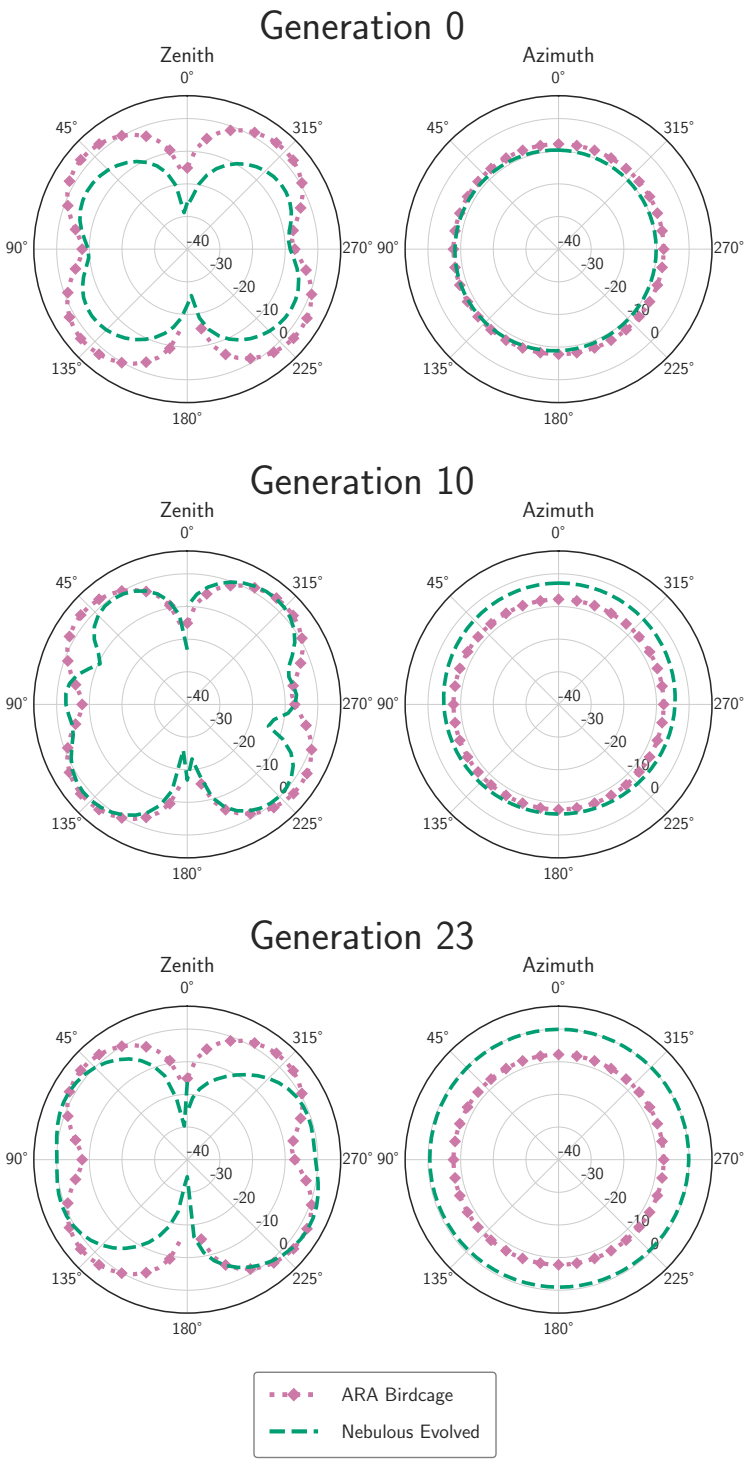

Figure 7. The gain patterns at 600 MHz of the most fit individual as of generations 0 (top), 10 (middle), and 23 (bottom). The ARA antenna gain pattern is overlaid in pink.

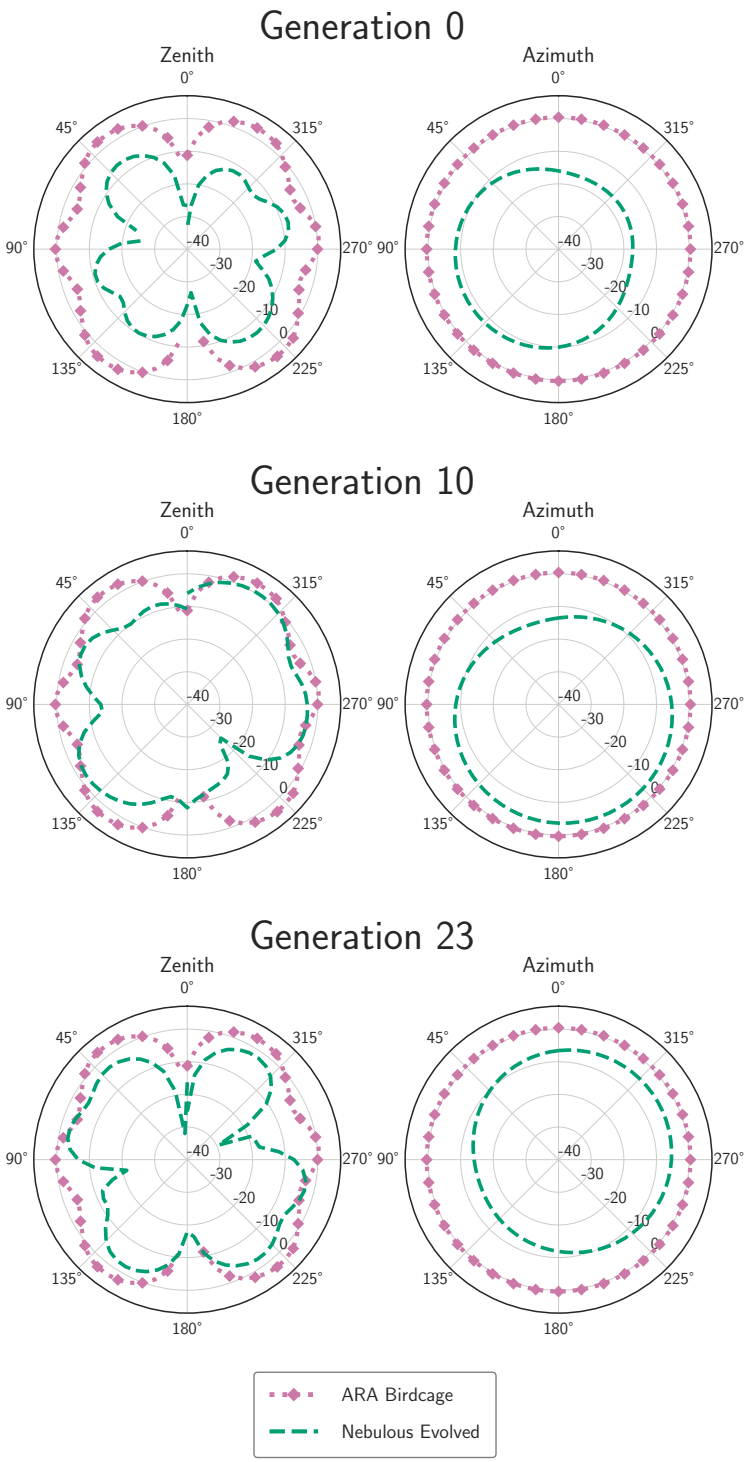

Figure 8. The gain patterns at 900 MHz of the most fit individual as of generations 0 (top), 10 (middle), and 23 (bottom). The ARA antenna gain pattern is overlaid in pink.

A. Physics Interpretation of Results

To further study the source of the improvements in performance of the evolved individuals, as well as validate their performance in terms of underlying physics, arrival directions of the simulated neutrinos detected by the ARA antenna design and the top-performing evolved antenna design were histogrammed. The same number of simulated neutrinos were thrown, 3×10^6, when evaluating each design.

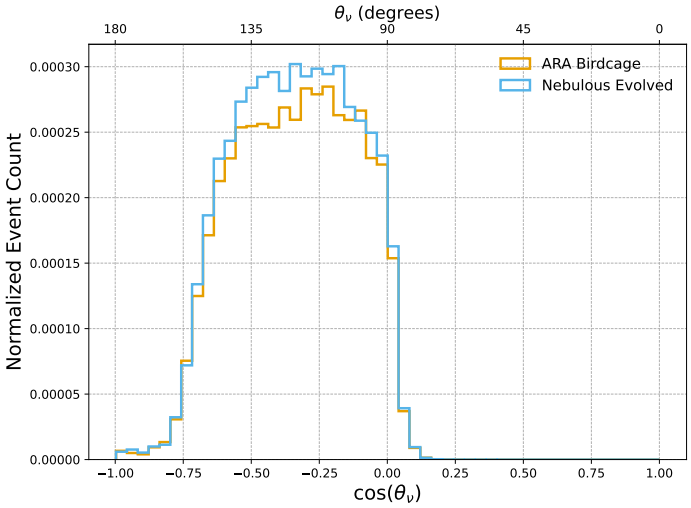

Figure 9. Histogram of the number of simulated neutrinos detected, binned by angle of neutrino incidence by the ARA bicone design and the top-performing design from the evolution (evaluation 8285).

Figure 9 displays a histogram of the arrival directions of detected simulated neutrinos, $\cos\theta_\nu$, for the two antenna designs. Both designs detect simulated neutrinos in the same range of angles, with the number of detected particles peaking in the same regions. However, the evolved design is seen to detect more events in most directions where the designs maintain sensitivity.

Figure 10 displays a similar histogram, showing the number of events detected binned by arrival direction of the RF signal, $\cos\theta_{RF}$, caused by the simulated neutrinos incident on the detector medium (antarctic ice). Again, it is seen that the two designs are sensitive to simulated events in the same angular ranges, with peak sensitivity also in similar directions. The evolved design is again seen to detect higher event counts at almost all angles where the antennas are sensitive to incident RF signals.

IV. Discussion

While the evolutionary algorithm found overall success on this problem, evolving using Monte Carlo simulations poses several challenges, particularly in steady-state evolutionary algorithms. High-performing individuals that score well when evaluated can continually propagate their genes through the population, even if their high

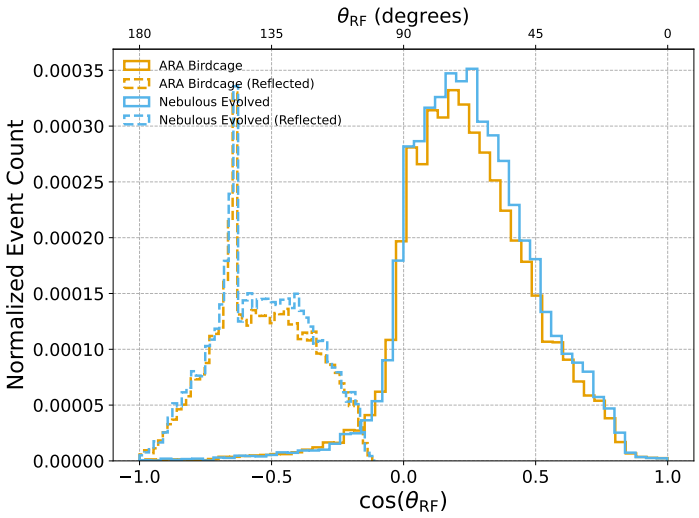

Figure 10. Histograms of the number of simulated neutrinos detected, binned by angle of radio signal incidence by the ARA bicone design and the top-performing design from the evolution (evaluation 8285).

performance was due to a statistical fluctuation as opposed to their genetic material. As a result, the population may stagnate and converge prematurely to a local optimum around these lucky performers.

Traditional approaches in evolutionary computation, such as re-evaluating individuals many times and taking the average, are not feasible with such a complex and expensive fitness function. Here, we combated these issues by running with a lower number of neutrinos used to evaluate individuals initially, and then increasing the number of neutrinos after approximately 6000 evaluations. This increase in neutrinos reduced potential error and punished any individuals that persisted through a lucky initial evaluation. A reduction in error later in the run still allowed for early and fast exploration of the parameter space while also encouraging fine tuning of the actual elite of the population late in the run.

Additionally, our use of ALPS and the injection operator work to combat the potential collapse of population diversity early in the run due to solutions benefiting from a statistical fluctuation in their fitness score. Injection continually adds new solutions to the population, which are protected in the younger layers. This approach prevents the population from homogenizing and allows for new innovations to spread and potentially out compete older individuals with deceptively high fitness.

V. Conclusion

This report presents an EA that can evolve antennas designs using science simulation software to evaluate fitness. XFdtd was used to determine the gain patterns of individual designs, which were in turn used by a Monte Carlo science simulation to

evaluate the antenna sensitivity. The algorithm was successful at producing antenna designs that exceed the sensitivity of currently deployed antennas.

VI. Future and Ongoing Work

The goal of the project is to be able to design a broad range of antennas by leveraging EAs used to evolve designs toward a science outcome using a Monte Carlo science simulation software. The current design capabilities showcased in this report are limited to dipole-like designs with driven antenna elements; due to the way the EA constructs antennas, the feed is restricted to a dipole-like structure. Recent design improvements have been made that expand the range of antenna designs that the algorithm is capable of achieving, namely designs with multiple feeds and/or the inclusion of passive elements. Tests validating the inclusion of these new design capabilities are currently in progress and will be showcased in a future IPN report. Including passive components can offer benefits such as impedance matching and radiation pattern shaping, which are crucial for optimizing antenna performance. To facilitate the creation of more intricate antenna geometries, we plan to expand the set of primitive building blocks used in the antenna construction process. Introducing additional primitives will enable the EA to combine a greater variety of components, potentially leading to innovative designs that enhance performance.

Improving the computational efficiency of our EA is another key focus area. We are working on optimizing the algorithm to reduce computation time without sacrificing the quality of the evolved designs. This includes refining selection methods, improving evolutionary operations, and utilizing parallel processing techniques to accelerate convergence. Techniques designed to be used when evolving under uncertainty will also be considered to improve the speed of the algorithm. In particular, dynamically adjusting the number of neutrinos simulated in each layer could help throw out bad solutions earlier and waste less resources on individuals with high fitness scores due to statistical fluctuations. In collaboration with our partners at Remcom, we are also exploring ways to improve the computational efficiency of XFdtd simulations, which are integral to evaluating antenna performance during the evolution process. By optimizing both our algorithm and the simulation software, we aim to significantly reduce the overall computational resources required.

Looking ahead, we plan to extend the algorithm to optimize arrays of antennas rather than individual units. Array optimization involves evolving the configuration and positioning of multiple antennas to maximize collective performance for UHE neutrino detection. This approach will allow us to design detector systems that consider interactions of multiple antennas and overall array effectiveness, potentially leading to breakthroughs in detection capabilities.

We also intend to integrate MOO into the EA, allowing for the simultaneous optimization of multiple science objectives, such as maximizing sensitivity across

different frequency bands while minimizing physical size or cost. This will enable us to identify antenna designs that offer the best trade-offs among various performance criteria, leading to more versatile and practical solutions for UHE neutrino detection experiments.

In addition, we are exploring the potential to incorporate origami-inspired folding techniques into antenna designs. The implementation of foldable structures could facilitate the development of deployable antennas that are compact during transport and expand to full size upon deployment. This capability is particularly valuable for space-based or remote installations where size and weight constraints are critical.

The advancements planned for the project have significant implications not only for UHE neutrino detection but also for the broader field of scientific instrumentation. By pushing the boundaries of antenna design through advanced evolutionary algorithms and incorporating new features and optimization techniques, we aim to enhance the sensitivity and effectiveness of future neutrino detection experiments. These efforts demonstrate the potential of heuristic optimization methods in advancing scientific research and may pave the way for their application in other areas of experimental physics and engineering.

Acknowledgments

The research was carried out at the Jet Propulsion Laboratory, California Institute of Technology, under a contract with the National Aeronautics and Space Administration (80NM0018D0004). The authors are grateful to the entire GENETIS collaboration for their prior work and continued assistance. We also thank Remcom for their support, especially Tarun Chawla, Walter Janusz, and Benjamin Hardy. The authors thank the ARA Collaboration for making available the AraSim simulation program used in this work.

References

[1] J. Rolla, B. Reynolds, J. Weiler, A. Connolly, R. Debolt, A. Machtay, B. Sipe, and D. Wells, "Design of 3d antenna geometries using genetic algorithms," *The Interplanetary Network Progress Report*, vol. 42-234, Jet Propulsion Laboratory, Pasadena, California, pp. 1–26, August 15, 2023.

[2] R. Luebbers, "XFDTD and beyond-from classroom to corporation," *2006 IEEE Antennas and Propagation Society International Symposium*, Albuquerque, New Mexico, pp. 119–122, 2006.

[3] J. Rolla, B. Reynolds, D. Wells, J. Weiler, A. Connolly, and R. Debolt, "Design of antennas from primitive shapes using genetic algorithms," *The Interplanetary Network Progress Report*, vol. 42-237, Jet Propulsion Laboratory, Pasadena, California, pp. 1–47, May 15, 2024.

[4] P. Allison et al., "First constraints on the ultra-high energy neutrino flux from a prototype station of the Askaryan Radio Array," *Astroparticle Physics*, vol. 70, pp. 62–80, October 2015, The AraSim repository can be found at https://github.com/ara-software/AraSim.

[5] F. Rothlauf, *Design of Modern Heuristics: Principles and Application*. Berlin, Germany: Springer, 2011.

[6] F. Tamjid, F. Foroughian, C. M. Thomas, A. Ghahreamani, R. Kazemi, and A. E. Fathy, "Toward high-performance wideband GNSS antennas-Design tradeoffs and development of wideband feed network structure," *IEEE Transactions on Antennas and Propagation*, vol. 68, no. 8, pp. 5796–5806, 2020.

[7] B. R. Rao, *GPS/GNSS Antennas*. Boston, Massachusetts: Artech House, 2013.

[8] J. J. H. Wang, "Antennas for global navigation satellite system (GNSS)," *Proceedings of the IEEE*, vol. 100, no. 7, pp. 2349–2355, 2012.

[9] A. Romero-Wolf, S. Vance, F. Maiwald, E. Heggy, P. Ries, and K. Liewer, "A passive probe for subsurface oceans and liquid water in Jupiter's icy moons," *Icarus*, vol. 248, pp. 463–477, 2015. https://www.sciencedirect.com/science/article/pii/S0019103514006009

[10] D. M. Schroeder, A. Romero-Wolf, L. Carrer, C. Grima, B. A. Campbell, W. Kofman, L. Bruzzone, and D. D. Blankenship, "Assessing the potential for passive radio sounding of Europa and Ganymede with RIME and REASON," *Planetary and Space Science*, vol. 134, pp. 52–60, 2016. https://www.sciencedirect.com/science/article/pii/S0032063316301465

[11] R. Prechelt, A. Romero-Wolf, P. Gorham, E. Costello, R. Ghent, and P. Lucey, "Radio detection of subsurface lunar ice via the Askaryan effect with the cosmic ray lunar sounder (CoRaLS)," *AGU Fall Meeting Abstracts*, New Orleans, Louisiana, December 2021.

[12] W. M. Farrell, M. D. Desch, and P. Zarka, "On the possibility of coherent cyclotron emission from extrasolar planets," *Journal of Geophysical Research: Planets*, vol. 104, no. E6, pp. 14 025–14 032, June 1999.

[13] P. Zarka, R. A. Treumann, B. P. Ryabov, and V. B. Ryabov, "Magnetically-driven planetary radio emissions and application to extrasolar planets," *Astrophysics and Space Science*, vol. 277, no. 1/2, pp. 293–300, June 2001.

[14] T. J. W. Lazio and W. M. Farrell, "Radio detection of extrasolar planets: Present and future prospects," *Proceedings of the 6th International Workshop on Planetary and Solar Radio Emissions*, Graz, Austria, pp. 603–610, 2006.

[15] E. Feenberg and H. Primakoff, "Interaction of cosmic-ray primaries with sunlight and starlight," *Physical Review*, vol. 73, no. 5, pp. 449–469, March 1948.

[16] J. E. Felten and P. Morrison, "Omnidirectional inverse Compton and synchrotron radiation from cosmic distributions of fast electrons and thermal photons," *Astrophysical Journal*, vol. 146, p. 686, December 1966.

[17] M. J. Rees, "Studies in radio source structure-III. Inverse Compton radiation from radio sources," *Monthly Notices of the Royal Astronomical Society*, vol. 137, no. 4, pp. 429–444, December 1967.

[18] G. R. Blumenthal and R. J. Gould, "Bremsstrahlung, synchrotron radiation, and Compton scattering of high-energy electrons traversing dilute gases," *Reviews of Modern Physics*, vol. 42, no. 2, pp. 237–271, January 1970.

[19] L. Feretti and G. Giovannini, "Diffuse cluster radio sources (review)," *Proceedings of the 175th Symposium of the International Astronomical Union*, Bologna, Italy, vol. 175, p. 333, January 1996.

[20] S. R. Furlanetto, S. P. Oh, and F. H. Briggs, "Cosmology at low frequencies: The 21 cm transition and the high-redshift Universe," *Physics Reports*, vol. 433, no. 4-6, pp. 181–301, October 2006.

[21] J. R. Pritchard and A. Loeb, "Evolution of the 21cm signal throughout cosmic history," *Physical Review D*, vol. 78, no. 10, p. 103511, November 2008.

[22] J. R. Pritchard and A. Loeb, "Constraining the unexplored period between the dark ages and reionization with observations of the global 21 cm signal," *Physical Review D*, vol. 82, no. 2, p. 023006, July 2010.

[23] A. Liu, J. R. Pritchard, M. Tegmark, and A. Loeb, "Global 21 cm signal experiments: A designer's guide," *Physical Review D*, vol. 87, no. 4, p. 043002, February 2013.

[24] O. Duzel, B. Saoud, I. Shayea, and G. N. Tulepova, "Antenna optimization based on genetic algorithm," *2024 IEEE 3rd World Conference on Applied Intelligence and Computing (AIC)*, Gwalior, India, pp. 511–517, 2024.

[25] P. Ghewari and V. Patil, "Advancements in microstrip patch antenna design using nature-inspired metaheuristic optimization algorithms: A systematic review," *Archives of Computational Methods in Engineering*, vol. 32, pp. 3687–3732, 2025.

[26] S. K. Goudos, D. E. Anagnostou, C. Kalialakis, P. Vasant, S. Nikolaou et al., "Evolutionary algorithms applied to antennas and propagation: Emerging trends and applications," *International Journal of Antennas and Propagation*, vol. 2016, 2016.

[27] B. Liu et al., "Optimization of the design of gas Cherenkov detectors for ICF diagnosis," *Nuclear Instruments and Methods in Physics Research Section A: Accelerators, Spectrometers, Detectors and Associated Equipment*, vol. 897, pp. 54–58, 2018.

[28] A. Liu, A. Bross, and D. Neuffer, "Optimization of the magnetic horn for the nuSTORM non-conventional neutrino beam using the genetic algorithm," *Nuclear Instruments and Methods in Physics Research Section A: Accelerators, Spectrometers, Detectors and Associated Equipment*, vol. 794, pp. 200–205, 2015.

[29] G. Oliveri, P. Rocca, L. Poli, M. Carlin, E. T. Bekele, A. De Matteis, and A. Massa, "Evolutionary strategies for advanced array optimization," *2011 IEEE International Symposium on Antennas and Propagation (APSURSI)*, Spokane, Washington, pp. 2441–2444, 2011.

[30] F. Grimaccia, M. Mussetta, A. Niccolai, and R. E. Zich, "Comparison of binary evolutionary algorithms for optimization of thinned array antennas," *2018 IEEE Congress on Evolutionary Computation (CEC)*, Rio de Janeiro, Brazil,, pp. 1–8, 2018.

[31] Q. Xu, S. Zeng, F. Zhao, R. Jiao, and C. Li, "On formulating and designing antenna arrays by evolutionary algorithms," *IEEE Transactions on Antennas and Propagation*, vol. 69, no. 2, pp. 1118–1129, 2021.

[32] G. Hornby et al., "Automated antenna design with evolutionary algorithms," *American Institute of Aeronautics and Astronautics*, Space 2006, San Jose, California, 2006.

[33] J. Rolla, A. Machtay, A. Patton, W. Banzhaf, A. Connolly, R. Debolt, L. Deer, E. Fahimi, E. Ferstle, P. Kuzma, C. Pfendner, B. Sipe, K. Staats, and S. A. Wissel, "Using evolutionary algorithms to design antennas with greater sensitivity to ultrahigh

energy neutrinos," *Physical Review D*, vol. 108, p. 102002, Nov 2023. https://link.aps.org/doi/10.1103/PhysRevD.108.102002

[34] G. S. Hornby, "Steady-state ALPS for real-valued problems," *Proceedings of the 11th Annual Conference on Genetic and Evolutionary Computation*, pp. 795–802, 2009. https://doi.org/10.1145/1569901.1570011

[35] ——, "ALPS: The age-layered population structure for reducing the problem of premature convergence," *Proceedings of the 8th Annual Conference on Genetic and Evolutionary Computation*, pp. 815–822, July 2006.

[36] J. Pan, S. Chitta, and D. Manocha, "FCL: A general purpose library for collision and proximity queries," *2012 IEEE International Conference on Robotics and Automation*, Saint Paul, Minnesota, pp. 3859–3866, 2012.

[37] RemCom, personal communication, 2022.

[38] *IEEE Standard for Definitions of Terms for Antennas*2014.

[39] I. Kravchenko, C. Cooley, S. Hussain, D. Seckel, P. Wahrlich, J. Adams, S. Churchwell, P. Harris, S. Seunarine, A. Bean et al., "RICE limits on the diffuse ultra-high energy neutrino flux," *Physical Review D*, vol. 73, no. 8, p. 082002, January 2006.

[40] J. Zhong, X. Hu, M. Gu, and J. Zhang, "Comparison of performance between different selection strategies on simple genetic algorithms," *International Conference on Computational Intelligence for Modelling, Control and Automation, and International Conference on Intelligent Agents, Web Technologies and Internet Commerce (CIMCA-IAWTIC'06)*, Vienna, Austria, pp. 1115–1121, 2005.

[41] A. Shukla et al., "Comparative review of selection techniques in genetic algorithm," *2015 International Conference on Futuristic Trends on Computational Analysis and Knowledge Management*, Greater Noida, India, 2015.

APPENDICES

I. Individual Genes and Genetic Algorithm Parameters

Table 3. Parameters used in genetic algorithm.

Category	Type	Parameters
General	Run	Num. Individuals, Num. Generations, Fitness Function, Target pattern, Steady-state flag, Forced diversity flag
	Individual	Max. Tree Depth, Max. Shapes, Shell thickness
	XFdtd	Frequency range, Frequency step
Shape	Cuboid	Shape allowed, Length, Width, and Height Ranges
	Sphere	Shape allowed, Radius Range
	Cylinder	Shape allowed, Radius, and Height Range
	Cone	Shape allowed, Radius 1, Radius 2, and Height Range
Selection Methods	Tournament	Percent of parents, Group Size
	Roulette	Percent of parents
	Rank	Percent of parents
Genetic Operators	Dim. Mutation	Percent of children, St. Dev. %
	Rotation Mutation	Percent of children, St. Dev. %
	Location Mutation	Percent of children, St. Dev. %
	Grow Mutation	Percent of children
	Prune Mutation	Percent of children
	Regen. Mutation	Percent of children
	Side Switch	Percent of children
	Gene Crossover	Percent of children
	Branch Crossover	Percent of children
	Reproduction	Percent of children
	Injection	Percent of children

Table 4. Primitive shape genes.

Gene	Values
Shape Type	Cuboid, Cylinder, Cone, Sphere
Dimensions	Varies by shape type (See Table 5)
Location	Cartesian coordinates of shape midpoint
Rotation	θ, ϕ
Connected From	Shape built from
Connected To	Side that shapes are attached to

Table 5. Dimensions for each shape type.

Shape Type	Dimension Genes
Cuboid	Length, Width, Height
Cylinder	Radius, Height
Cone	Inner Radius, Outer Radius, Height
Sphere	Radius

II. Additional Results

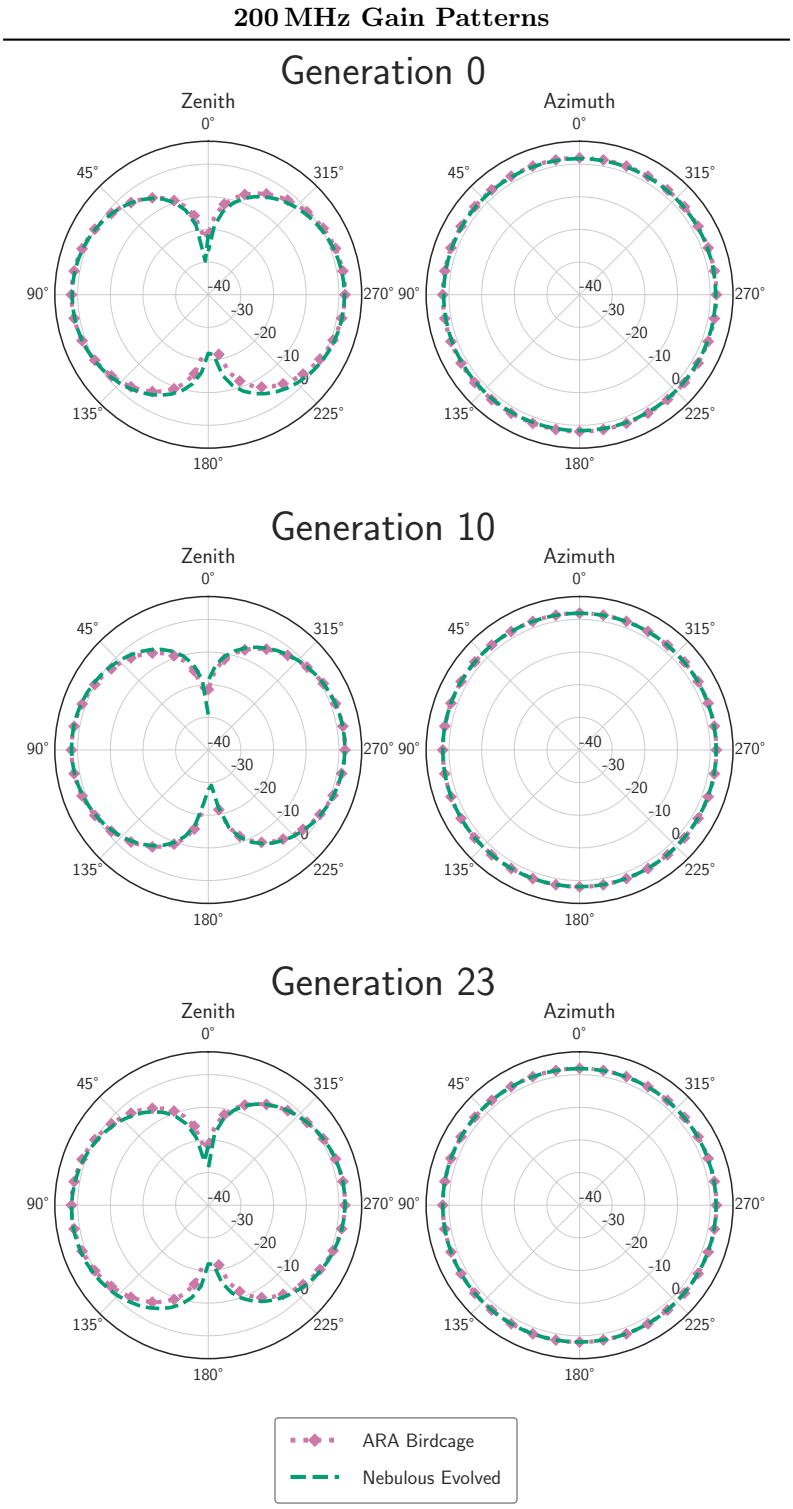

Figure 11. The gain patterns at 200 MHz of the most fit individual as of generations 0 (top), 10 (middle), and 23 (bottom). The ARA antenna gain pattern is overlaid in pink.

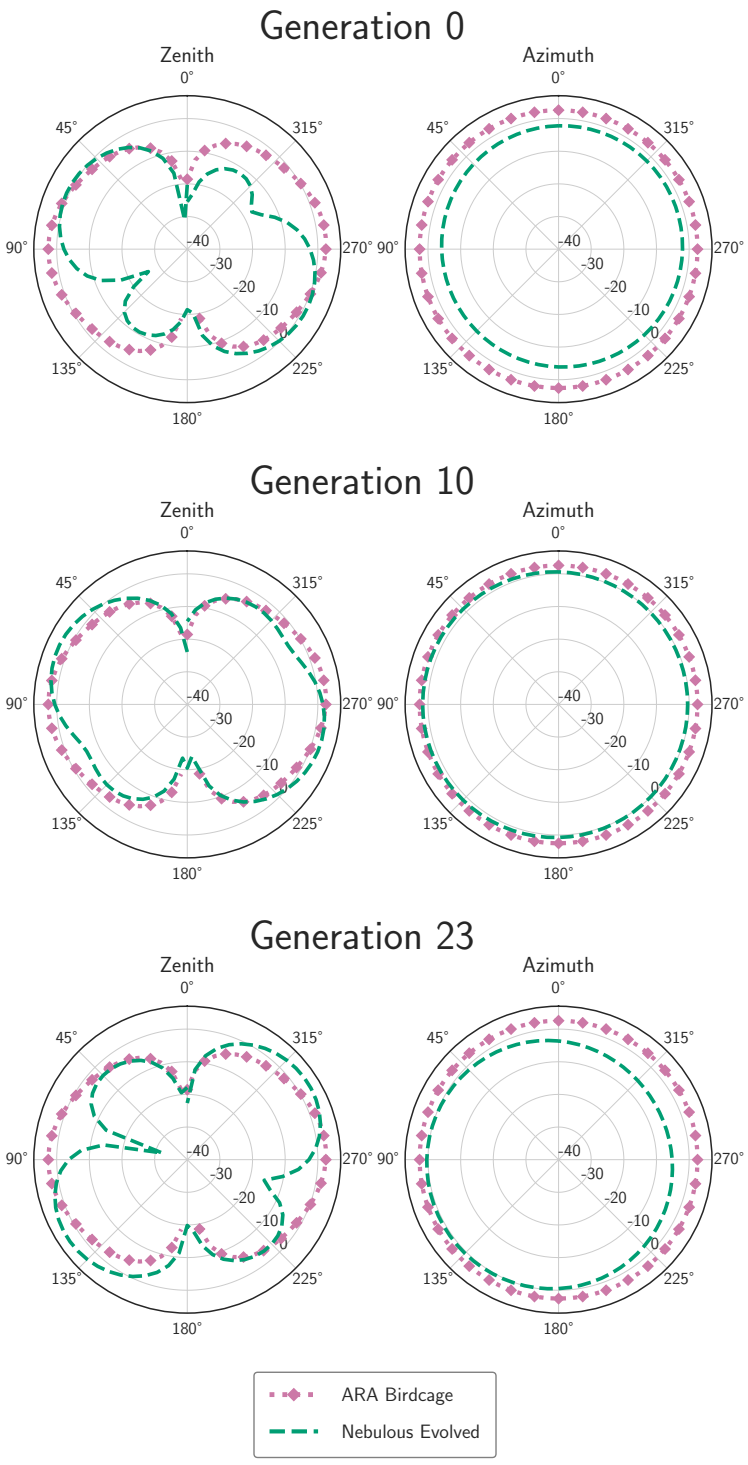

Figure 12. The gain patterns at 400 MHz of the most fit individual as of generations 0 (top), 10 (middle), and 23 (bottom). The ARA antenna gain pattern is overlaid in pink.

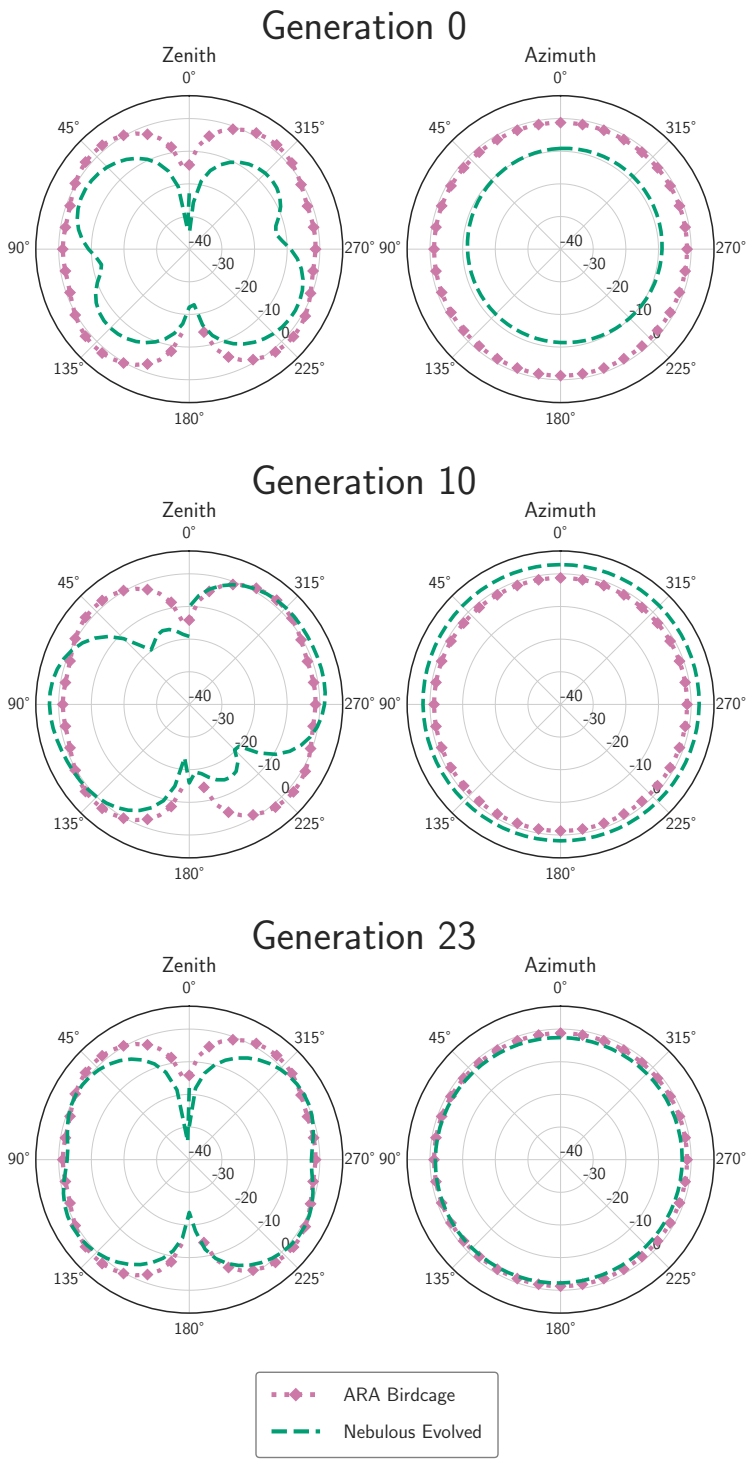

Figure 13. The gain patterns at 500 MHz of the most fit individual as of generations 0 (top), 10 (middle), and 23 (bottom). The ARA antenna gain pattern is overlaid in pink.

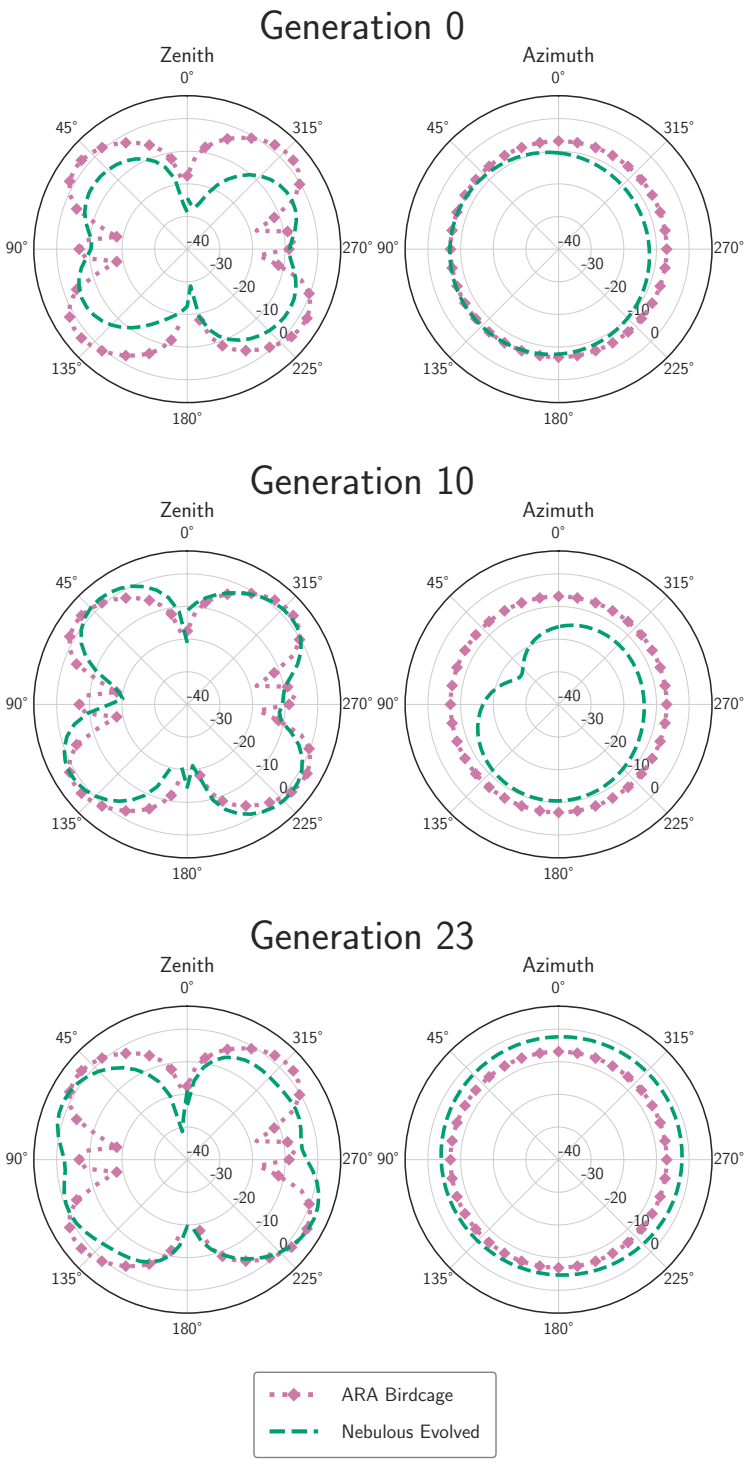

Figure 14. The gain patterns at 700 MHz of the most fit individual as of generations 0 (top), 10 (middle), and 23 (bottom). The ARA antenna gain pattern is overlaid in pink.

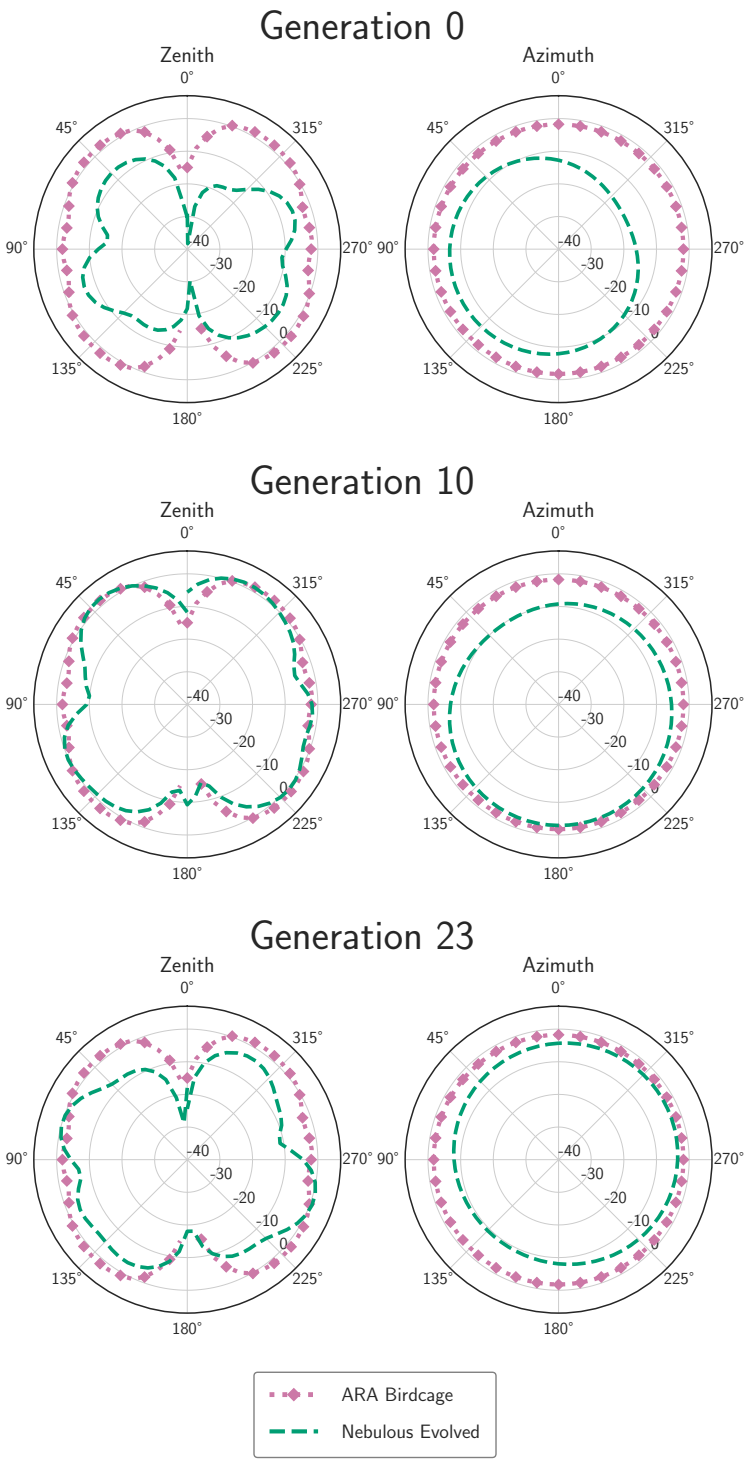

Figure 15. The gain patterns at 800 MHz of the most fit individual as of generations 0 (top), 10 (middle), and 23 (bottom). The ARA antenna gain pattern is overlaid in pink.

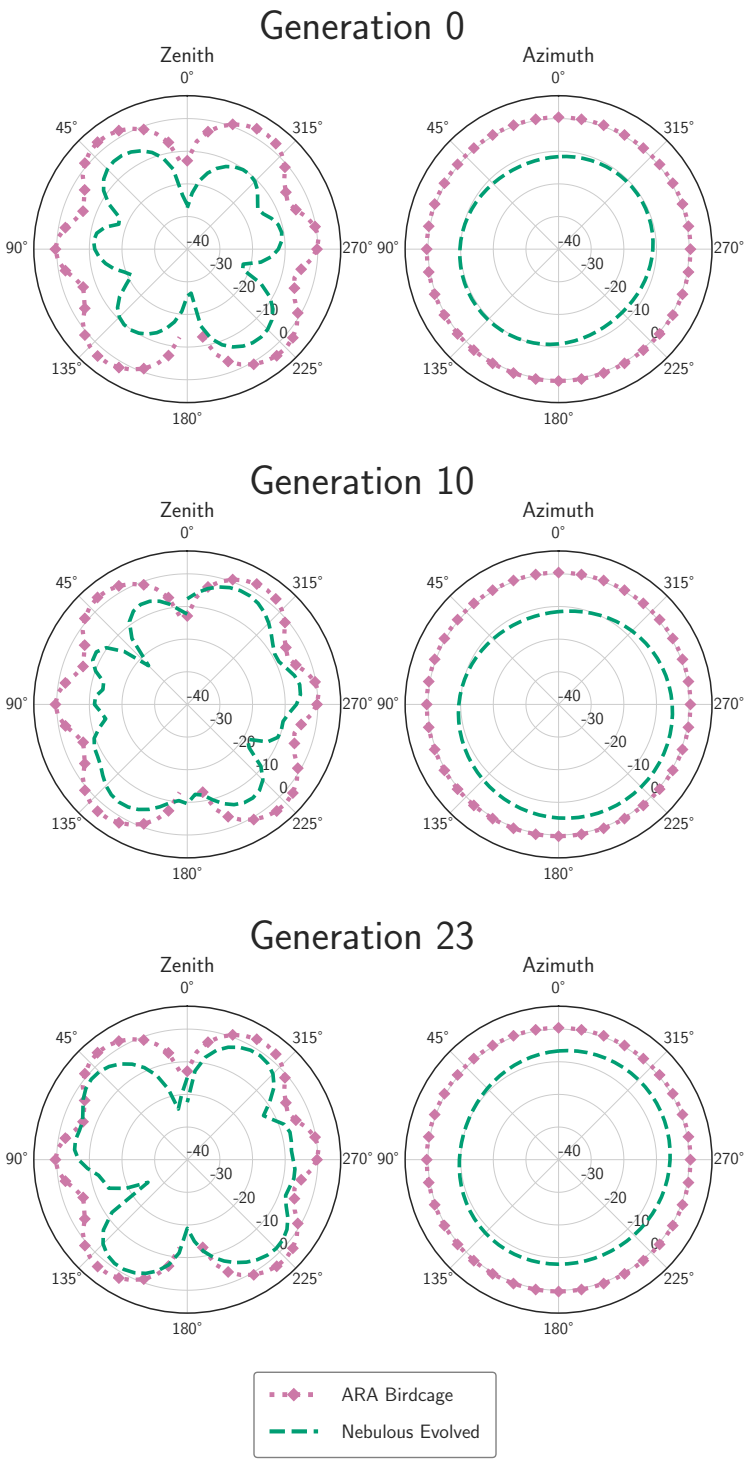

Figure 16. The gain patterns at 1000 MHz of the most fit individual as of generations 0 (top), 10 (middle), and 23 (bottom). The ARA antenna gain pattern is overlaid in pink.